

# SIMULATION

<http://sim.sagepub.com>

---

## Computer Simulation of 3-D Liquid Transport in Fibrous Materials

D. Lukas, V. Soukupova, N. Pan and D. V. Parikh

*SIMULATION* 2004; 80; 547

DOI: 10.1177/0037549704047307

The online version of this article can be found at:  
<http://sim.sagepub.com/cgi/content/abstract/80/11/547>

---

Published by:



<http://www.sagepublications.com>

On behalf of:



Society for Modeling and Simulation International (SCS)

**Additional services and information for *SIMULATION* can be found at:**

**Email Alerts:** <http://sim.sagepub.com/cgi/alerts>

**Subscriptions:** <http://sim.sagepub.com/subscriptions>

**Reprints:** <http://www.sagepub.com/journalsReprints.nav>

**Permissions:** <http://www.sagepub.co.uk/journalsPermissions.nav>

**Citations** <http://sim.sagepub.com/cgi/content/refs/80/11/547>

# Computer Simulation of 3-D Liquid Transport in Fibrous Materials

**D. Lukas**

**V. Soukupova**

Technical University of Liberec  
Liberec, Czech Republic

**N. Pan**

Division of Textiles and Clothing  
Biological and Agricultural Engineering Department  
University of California, Davis  
*npan@ucdavis.edu*

**D. V. Parikh**

South Regional Research Center  
New Orleans, LA

Liquid movement in 3-D fibrous materials is studied in this article by means of Monte Carlo simulation based on the Ising model with so-called Kawasaki kinetics. Computer simulation algorithms are then developed in accordance with the standard liquid wicking rate tests from both EDANA and INDA, and the simulation results provide information of liquid wicked into computer-generated fiber assemblies as a function of time. The work focuses mainly on the relationship between fiber orientation and the liquid wicking rate, while other geometrical parameters of the fiber mass remain fixed. Furthermore, this simulation also presents dynamic data of both liquid mass uptake and energy changes of the system. The results are in agreement with known experimental evidence.

**Keywords:** Liquid transport, fibrous materials, 3-D Ising model, wetting rate, fiber orientation

## 1. Introduction

A flow involving more than a single phase is classified as multiphase or nonhomogeneous, such as liquid flows in porous fiber media, and we are interested in the dynamics of the evolving macroscopic interface between the distinct phases during such nonhomogeneous flows in a fiber mass. The dynamics of such flow are dominated by surface tensions, porous media anisotropy and nonhomogeneity, fiber volume fraction, and fiber wetting behaviors. The uncertain structural conditions in fibrous media, including the susceptibility to even small loads, as well as the tortuous connectivity of their open pores and poorly defined boundaries, result in complex local nonhomogeneous flows and interfacial evolution [1]. This complexity, in many cases, becomes prohibitive for the development of analytical theories describing these phenomena.

The wetting and wicking of fiber mass constitute a class of flows that have critical scientific and practical signif-

icance, on which technologies such as fiber lubricating and processing, fiber-reinforced composite manufacturing, and fiber web bonding and dyeing are based. Wetting and wicking behaviors of many consumer products, such as baby diapers, female hygiene products, and sport and other protective garments, are critical in determining their commercial success.

The field of nonhomogeneous flows has become an active area for systematic research since the mid-19th century. The basic theory was the equation of capillarity given by Young [2] and Laplace [3]. One of the earliest works is that of Lamb [4], published in 1879, containing the topic of the motion of solids through liquids. In 1970s, some pioneering works about the dynamics of liquid spreading on solids were published; Huh and Scriven [5] suggested a singularity in the dissipation in such flows. A useful distinction was revealed between simple fluids: for example, liquid spreads by a “rolling motion” [6], whereas polymeric melts often tend to slip on a solid surface [7]. More recently, de Gennes [8] published a review on wetting research.

The first attempt to understand the capillary-driven nonhomogeneous flows for practical applications was made by Lucas [9] and Washburn [10]. The Lucas–Washburn theory

has been used in and further developed for the textile area by a few authors. Chatterjee [11] dealt with these kinds of flows in dyeing. Pillai and Advani [12] conducted an experimental study of the capillarity-driven flow of viscous liquids across a bank of aligned fibers. Hsieh [13] discussed wetting and capillary theories and applications of these principles to the analysis of liquid wetting and transport in fibrous materials. Several techniques employing fluid flow to characterize the structure of fibrous materials were presented in Hirt et al. [14] as well. Lukas and Soukupova [15] carried out a data analysis to test the validity of the Lucas–Washburn approach for some fibrous materials and obtained a solution for the Lucas–Washburn equation, including the gravity term.

Nonhomogeneous flows have also been studied using stochastic simulation. Manna, Herrmann, and Landau [16] presented a stochastic simulation that generates the shape of a 2-D liquid drop, subject to gravity, on a wall. The system was based on the so-called Ising model with Kawasaki dynamics. They located a phase transition between a hanging and a sliding droplet. Lukkarinen [17] studied the mechanisms of a fluid droplet spreading on flat solids and found that at first, the spreading is of nearly linear behavior with time, and the liquid precursor film spreading is dominated by the surface flow on the bulk droplet of a solid; later, however, the dynamics of liquid spreading are governed by a square root of time. A similar study of fluid droplet spreading on a porous surface was recently reported too [18]. The first attempt to simulate liquid wetting dynamics in fiber structures using the Ising model was done by the present authors [19, 20], followed by Zhong, Ding, and Tang [21, 22], although the simulation was restricted to 2-D systems only.

In this article, we apply a 3-D Ising stochastic method to the simulation of wicking dynamics in a system of fibers with a given orientation. The benefit of using 3-D simulation is to provide a more realistic model to actual fibrous systems, where a linear object (a fiber) does not create a serious hindrance for a liquid transport but can easily be evaded. Next, there are substantial differences of flows in 2-D and 3-D spaces, even for such an elementary case as the viscous flow in a straight tube (the Hagen–Poiseuille flow). In both 2-D and 3-D instances, the velocity field profile is parabolic, although parameters of such parabolas are more diverse in the 2-D case than in the 3-D one. There is no reason to believe that such differences disappear for the liquid transport phenomena when dealt with by using stochastic approaches.

The chosen method enables us to investigate wetting and wicking phenomena as well as to predict system parameters that are comparable with experimental ones at the macroscopic level. One of the examples is the wicking rate—the quantity that can be measured, simulated, and theoretically derived from the Lucas–Washburn theory. The wicking rate in fibrous systems is heavily influenced by several complex geometrical parameters, as mentioned previously. Hence we have concentrated the present

work exclusively on one aspect—the effect of a fiber mass orientation. Other morphological features, such as heterogeneity, fiber volume fraction, fiber aspect ratio, fiber curl, and fiber surface geometry, are kept as constants in the bulk of modeled specimens. All fibers were represented by strictly linear geometry. In other words, the main subject in this article is a detailed study of the relationship between the wicking rate and fiber orientation.

## 2. On the Lucas–Washburn Theory

In demonstrating the necessity of, and in comparing with, our new technique, it is deemed desirable to provide a brief yet thorough recount of the existing theories.

For both scientific and practical purposes, the so-called wicking (or absorbency) rate is of great interest. The European Disposables and Nonwovens Association (EDANA) and the International Nonwovens and Disposables Association (INDA) recommended tests to measure the vertical speed at which the liquid is moving upward in a fabric as the capillarity of the test material. The vertical rate of absorption is measured from the edges of the test specimen strips suspended in a given liquid source. The resultant report of the test contains a record of capillary rising heights after the time of 10, 30, and 60 sec (and even 300 sec, if required). Gupta [23] defined the absorbency rate as the quantity that is characterized based on a modification of the Lucas–Washburn equation, and he then modified it to apply to a flat, thin circular fabric on which fluid diffuses radially outward.

Miller and Friedman [24] introduced a technique for monitoring absorption rates for materials under compression. Their Liquid/Air Displacement Analyser (LADA) measures the rate of absorption by recording changes of the liquid weight when liquid is sucked into a flat textile specimen connected to a liquid source.

A more scientific definition of the wicking rate is based on the Lucas–Washburn theory. This simple theory deals with the rate at which a liquid is drawn into a circular tube via capillary action. Such a capillary is a grossly simplified model of a pore in a real fibrous medium with a highly complex structure [25]. The theory is actually a special form of the Hagen–Poiseuille law [26] for laminar viscous flows. According to this law, the volume  $dV$  of a Newtonian liquid with viscosity  $\mu$  that wets through a tube of radius  $r$  and length  $h$  during time  $dt$  is given by the relation

$$\frac{dV}{dt} = \frac{\pi r^4 (p_1 - p_2)}{8h\mu}, \quad (1)$$

where  $p_1 - p_2$  is the pressure difference between the tube ends. The pressure difference here is generated by the capillarity force and the gravitation. The contact angle of the liquid against the tube wall is denoted as  $\theta$ , and the parameter  $\beta$  is the angle between the tube axis and the vertical direction shown in Figure 1. The capillary pressure  $p_1$  has the value

$$p_1 = \frac{2\gamma \cos \theta}{r}, \quad (2)$$

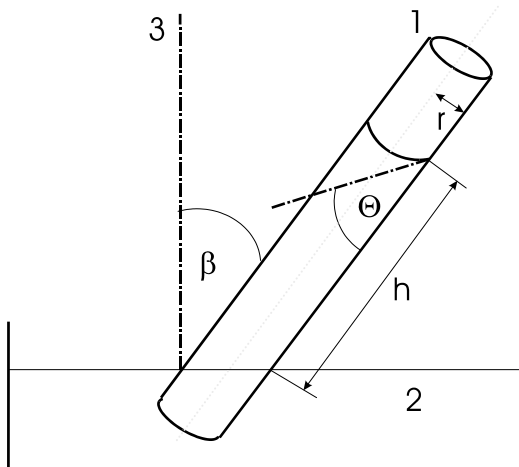


**Figure 1.** A tube (1) of a radius  $r$  is suspended in a liquid source (2). The distance traveled by the liquid along the capillary axis is  $h$ . The angle  $\theta$  is the contact angle between the liquid surface and the capillary wall, while  $\beta$  denotes the angle between the tube and the vertical axis (3).

while the hydrostatic pressure  $p_2$  is

$$p_2 = h\zeta g \cos \beta, \quad (3)$$

where  $\gamma$  denotes the liquid surface tension,  $\zeta$  is liquid density,  $g$  is the gravitational acceleration, and  $h$ , in this case, is the distance traveled by the liquid measured from the reservoir along the tube axis. This distance obviously is the function of time,  $h = h(t)$ , for a given system. When we substitute the quantities  $p_1$ ,  $p_2$ , and  $h(t)$  into equation (1), expressing the liquid volume in the capillary  $V$  as  $\pi r^2 h$ , we obtain the following Lucas–Washburn equation:

$$\frac{dh}{dt} = \frac{r\gamma \cos \theta}{4\mu h} - \frac{r^2 \zeta g \cos \beta}{8\mu}. \quad (4)$$

For a given system as shown in Figure 2a, parameters such as  $r$ ,  $\gamma$ ,  $\theta$ ,  $\mu$ ,  $\zeta$ ,  $g$ , and  $\beta$  remain constant. We can then reduce the Lucas–Washburn equation (4) by introducing two constants,

$$K' = \frac{r\gamma \cos \theta}{4\mu} \text{ and } L' = \frac{r^2 \zeta g \cos \beta}{8\mu}, \quad (5)$$

into a simplified version,

$$\frac{dh}{dt} = \frac{K'}{h} - L'. \quad (6)$$

The above relation is a nonlinear ordinary differential equation that is solvable only after ignoring the parameter  $L'$ ; this has a physical interpretation when either the liquid penetration is horizontal ( $\beta = 90^\circ$ ), or  $r$  is small, or the

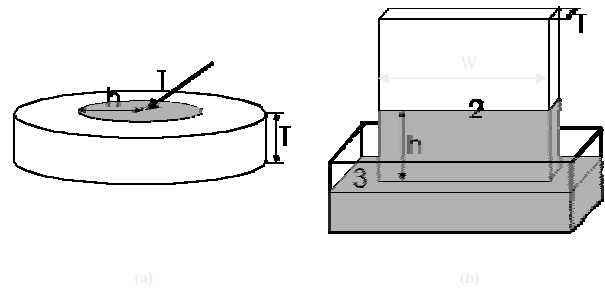


**Figure 2.** Two different experimental arrangements for wicking (absorbency) rate measurement: (a) liquid source initiates in the center of a flat specimen and is spread radially outward, and (b) liquid ascends in a specimen perpendicular to the reservoir liquid surface

rising liquid height  $h$  is low that  $\frac{K'}{h} \gg L'$  or  $L' \rightarrow 0$ , and the effects of the gravitation field are negligible and the acceleration  $g$  vanishes. The Lucas–Washburn equation (6) could thus be solved with ease:

$$h = \sqrt{2K't}. \quad (7)$$

The result satisfies the initial condition  $h = 0$  for  $t = 0$ .

Now we turn our attention back to Gupta's approach to the wicking rate [21], where a fluid from a point source in the center of a substrate spreads radially outward, instead of the ascending liquid front in a fibrous substrate partially dipped into a liquid, as illustrated in Figure 2.

It is useful now to transfer the Lucas–Washburn equation into a modified version by replacing the distance  $h$  with liquid mass uptake  $m$ . Such a transition is described in detail in Ford [27] and Hsieh [28]. This manipulation does not influence the fundamental shape of equation (7) because the relationship between  $h$  and  $m$  is linear for a circular tube of fixed cross-section. Furthermore, for the radial spreading, liquid mass is  $m_R = \pi h^2 T \zeta V_L$  and the ascending liquid front  $m_A = whT \zeta V_L$ , where  $T$  is the thickness of the substrate, and  $V_L$  is the liquid volume fraction inside the substrate of width  $w$ .

For the radial liquid spreading in a flat textile specimen, we can then write using equation (7)

$$Q = \frac{m_R}{t} = 2\pi K'T \zeta V_L, \quad (8)$$

where  $Q$  is the liquid wicking (absorbency) rate used by Gupta [23], which is independent of time during the spreading process.

Let us now substitute liquid mass uptake  $m_A$  into the original Lucas–Washburn equation (6), with the result as follows:

$$\frac{dm_A}{dt} = \frac{K}{m_A} - L. \quad (9)$$

The new constants  $K$  and  $L$  are

$$K = (wT\zeta V_L)^2 K', \quad L = wT\zeta V_L L'. \quad (10)$$

It is obvious that the constant  $K$  in the modified Lucas–Washburn equation (9) is proportional to the wicking (absorbency) rate  $Q$  that is defined in (8), and from (8) and (10), it follows that  $Q = \frac{2\pi}{w^2 T \zeta V_L} K$ . Hence, the parameter  $K$  can be used as a measure of the spreading wicking rate  $Q$  in the experiments when a fabric is hung vertically into a liquid. The values of  $K$  and  $L$  can be derived from the slope and intercept of the  $dm_A/dt$  versus  $1/m_A$ , as mentioned in Miller and Jansen [29].

On the other hand, equations (6) and (9) can be solved in terms of functions  $t(h)$  or  $t(m_A)$  without dropping the gravity term  $g$ , as shown in Lukas and Soukupova [15]. For the liquid mass uptake Lucas–Washburn equation (9), one obtains for the ascending liquid front the relation

$$t(m_A) = -\frac{m_A}{K} - \frac{K}{L^2} \ln\left(1 - \frac{L}{K} m_A\right). \quad (11)$$

Conversely, however, we are unable to acquire the inverse solution,  $m_A(t)$ , using the common functions.

The Lucas–Washburn approach presents an approximate but effective tool to investigate the wicking and wetting behavior of textiles despite their complicated, noncircular, nonuniform, and nonparallel structure of the pore spaces. It has been shown that equations (6) and (9) hold for a variety of fibrous media, including paper and textile materials [25, 30] and 3-D pads. Nevertheless, this theory is unable to deal with issues such as the influence of structure (e.g., fiber orientation and deformation on the wetting and wicking behavior of fibrous media). Therefore, the development of more robust techniques is desirable in this area, and the following is just such an attempt.

### 3. A 3-D Ising Model for Liquid–Fiber Mass Interaction

In this section, we develop the idea of using Monte Carlo simulation based on the Ising model for a description of the wetting and wicking phenomena in fibrous media. The idea was first introduced by us [19], albeit focused on a 2-D Ising model.

We introduce here a 3-D Ising model, incorporated with the stochastic dynamics and the method of importance sampling, which enables us to interpret the model outputs in terms of wicking dynamics. The essential principle of this model is based on the discretization of the whole system of a fibrous mass, a liquid source, and a wetting configuration at any given moment. The continuous media in the system, including the solid, liquid, and gas, are all divided as assemblies of individual cells occupied by the respective medium so that such a discrete system of cells can be manipulated more easily in a computer. The liquid wicking simulations are then set up from the initial configuration of

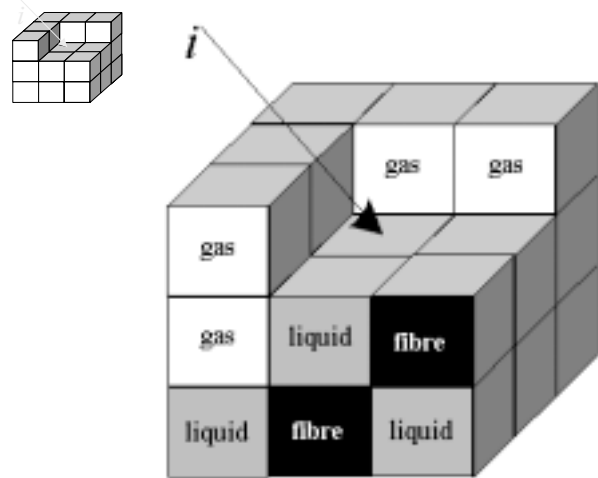


**Figure 3.** A cell  $i$  in the center to form a supercube with its neighboring cells. On the front surface, we can see various kinds of media that occupy the cells: the white color denotes the air, the grey color denotes the liquid, and fiber cells are black.

the liquid layer into which the fiber mass with a predefined fiber orientation is in part vertically dipped, absorbing the liquid.

Statistical physics in general deals with systems with many degrees of freedom. These degrees of freedom, in our case, are represented by the so-called Ising variables. We assume that we know the Hamiltonian (i.e., the total internal energy) of the system. The problem is computing the “average” or equilibrium macroscopic parameters observable (e.g., energy and liquid mass uptake) for a given initial system configuration. Moreover, we will monitor the kinetics/dynamics of the system so as to simulate the wicking behavior with time.

#### 3.1 The Ising Variables and the System Hamiltonian

The Ising model system used here consists of a rectangular simulation box of size  $W \times H \times L$  (width  $\times$  height  $\times$  length) subdivided into numerous lattice cells. Each cell is occupied by just one type of the media: gas, liquid, or fiber. The cells interact with their neighbors via the energy exchange. A neighborhood is formed by 26 cells arranged into a super-cube that surrounds the cell in the center, as seen in Figure 3. The exchange energy value depends on the types of interactions.

To make the description concise and more suitable for computer processing, we locate the lattice cells using indices  $i$  and  $j$  and designate a cell entity by the Ising variable or spin  $S_i$ . Indices  $i$  and  $j$  may vary in the range  $i, j \in \{1, 2, \dots, N\}$ , where  $N$  is the total number of cells. We set  $S = 0$  when a cell is occupied by gas,

**Table 1.** Exchange of energy values  $J(S_i, S_j)$  between two interacting cells

Interacting Cells	Gas, $S_j = 0$	Liquid, $S_j = 1$	Fiber, $S_j = 2$
Gas, $S_i = 0$	$J(0,0) = -40$	$J(0,1) = 5$	$J(0,2) = 20$
Liquid, $S_i = 1$	$J(1,0) = 5$	$J(1,1) = -26$	$J(1,2) = -30$
Fiber, $S_i = 2$	$J(2,0) = 20$	$J(2,1) = -30$	$J(2,2) = 0$

$S = 1$  by liquid, and  $S = 2$  by fiber. The exchange energy  $J$  is then a symmetrical function of two Ising variables,  $J(S_i, S_j) = J(S_j = S_i)$ . The possible energy values between two interacting cells are assigned as shown in Table 1.

There are nine possible combinations of pairs for the three kinds of Ising variables. However, the allowable combinations reduce to six due to the symmetry. Furthermore, because fiber structure or fiber cells are not movable during the simulation, the interaction energy value  $J(2, 2)$  does not play a role in the model and is hence set to 0.

Each isolated system tends to minimize its total internal energy, which is why we can expect the attraction of cells with low-exchange energy and the repulsion of ones with high-exchange energy. Values  $J(S_i, S_j)$  have been chosen to ensure such behavior by encouraging the aggregation of gas cells and liquid ones, respectively, whereas the liquid cells will preferably adhere, based on the assigned energy values reflecting the physics, to fibers instead of gas cells.

The presence of gravity is represented by a uniform field  $g$ . We assume that the gravity field interaction is significant only for liquid cells; the influence of the mass of both fiber and gas is smaller enough to be neglected. The gravity potential of a liquid particle of mass  $m$  in the cell  $I$ , located at the  $h_i$ th level of the lattice along the vertical axis  $H$ , is  $mgh_i$ . With these results, we can write the system Hamiltonian  $\Xi$  (total energy) as

$$\Xi = \sum_{(i,j)} J(S_i, S_j) + \sum_{(i)} mgh_i, \quad (12)$$

where  $\sum_{(i,j)}$  means that each cell couple is counted one time, and the sum  $\sum_{(i)}$  applies to the liquid cells only.

### 3.2 Importance Sampling

The model microscopic dynamics are governed by a stochastic (Monte Carlo) process. The dynamics are realized through the so-called importance sampling process proposed by Metropolis et al. [31]. These authors suggested constructing a Markov process in which each state or configuration of the model  $\mathbf{x}_{l+1}$  is evolved from the previous state  $\mathbf{x}_l$  via suitable transition probability  $W(\mathbf{x}_l \rightarrow \mathbf{x}_{l+1})$ . Here, the vector  $\mathbf{x}$  in the phase space stands for a set of Ising variables describing the considered degree of freedom—for example,  $\mathbf{x} = (S_1, S_2, \dots, S_N)$ —so the system Hamiltonian is a function of the state  $\mathbf{x}$  (i.e.,  $\Xi = \Xi(\mathbf{x})$ ). Again, in

our case, the initial system configuration is represented by a thin liquid layer at the bottom of the simulation box that coexists with a rigid fiber system. The frequently used choice for transition probability values is, according to Binder [32],

$$W(\mathbf{x}_l \rightarrow \mathbf{x}_{l+1}) = \frac{1}{\tau} e^{(-\delta \Xi/kT)} \text{if } \delta \Xi > 0,$$

$$W(\mathbf{x}_l \rightarrow \mathbf{x}_{l+1}) = \frac{1}{\tau} \text{otherwise}, \quad (13)$$

and parameters  $k$  and  $T$  in (13) denote the Boltzmann constant and temperature, while arbitrary factor  $\tau$  is a unit of the “Monte Carlo time” when the Monte Carlo process is interpreted dynamically [33]. The state exchange  $\mathbf{x}_l \rightarrow \mathbf{x}_{l+1}$  clearly depends on the energy difference after and before the exchange,

$$\Delta \Xi = \Xi(\mathbf{x}_{l+1}) - \Xi(\mathbf{x}_l). \quad (14)$$

With this choice of the transition probability, the distribution function  $P(\mathbf{x}_l)$  of states generated by this Markov process ( $\mathbf{x}_l \rightarrow \mathbf{x}_{l+1} \rightarrow \mathbf{x}_{l+2} \rightarrow \mathbf{x}_{l+3} \rightarrow \dots \rightarrow \mathbf{x}_{l+M}$ ) approaches, as  $M \rightarrow \infty$ , the equilibrium distribution  $P_{eq}(\mathbf{x}_{l+M})$  for a canonical ensemble in thermal equilibrium

$$P_{eq}(\mathbf{x}_{l+M}) = \frac{1}{Z} \exp(-\Xi(\mathbf{x}_{l+M})/kT), \quad (15)$$

where  $Z$  is the partition function as defined in Binder [32].

The explanation for this asymptotic convergence of the Markov chain of states to the equilibrium (steady-state) distribution  $P_{eq}$  is described in Binder and Heermann [34]. The procedure realizing the transition through the phase space set of points  $\{\mathbf{x}_l, \mathbf{x}_{l+1}, \mathbf{x}_{l+2}, \dots\}$  is called the *importance sampling* [36].

### 3.3 The Algorithm of the Computer Simulation

For our simulation, we set up a simple cubic lattice of size  $37 \times 300 \times 150$  ( $W \times H \times L$ ) with a total number of cells  $N = 1,665,000$  and free boundary conditions. The specification of an initial spin cell configuration is the following: the first 10 bottom layers  $h_i \in \{0, \dots, 9\}$  are immersed in a liquid pool, with Ising variables  $S_i = 1$ , and the rest of the lattice space is filled by gas spins so that  $S_i = 0$ .

The direction of the fiber is determined by two angles,  $\beta$  and  $\alpha$ , which contain the unit vector  $\mathbf{a}$  with the axis  $H$

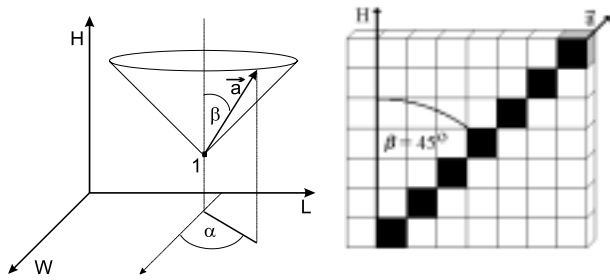


**Figure 4.** A fiber system is generated via the location of its origin  $o$  of a fiber containing a unit vector  $\mathbf{a}$  inside the simulation box  $W \times H \times L$ . On the right-hand side is a thin section of the simulation box (one cell thick) with a part of a fiber with the deflection angle  $\beta = 45^\circ$ .

and its projection in the horizontal ( $WL$ ) plane with the axis  $W$ . The orientation of  $\mathbf{a}$  can be chosen up or down the line, determined by the couple of angles  $(\alpha, \beta)$ . The vertical cross section of each fiber consists of one fiber cell only.

The fibrous mass is then created by the generation of individual random lattice cells as the origins of fibers. Then, a vector  $\mathbf{a}$  with a given direction  $\beta$ , as well as a uniform azimuth  $\alpha$  of the projection of  $\mathbf{a}$  via a random-number generator onto the horizontal  $W - L$  plane (see Fig. 4), is used to generate the fiber directions. Each fiber is defined as an abscissa with an equal probability up or down along the vector  $\mathbf{a}$  with the starting point in the fiber origin. The fiber length is equal to 50 lattice cell length, and diameter is equal to 1 lattice cell. The total number of fibers was chosen ( $M = 10,000$ ). Fibers thus generated are arranged throughout the cubic lattice so that they can be considered as chains of the cells they occupied (i.e., the fiber cells). The average fiber volume density  $V_f$  hence equals the fraction of fiber cells with respect to the total number of cells  $N$  [35]. Simulations were carried out for  $V_f = 0.22$ . After creation of the initial spin cell configuration, the simulation is conducted by repeating the following six steps:

1. Select two lattice cells  $i$  and  $j$  at which the Ising variables  $S_i$  and  $S_j$  are considered for exchange ( $S_i \rightarrow S_j$  and  $S_j \rightarrow S_i$ ). The spin  $S_i$  has to contain liquid, and  $S_j$  must be filled by gas. Moreover, both spins have to be located on the interface between liquid and gas. The liquid interface cell is defined as the one whose neighborhood consists of at least one gas cell. Correspondingly, the gas interface cell has in its neighborhood at least one liquid cell. This type of Ising variable exchange is called long-range Kawasaki spin exchange kinetics [36].
2. Compute the energy change  $\Delta E$ , defined in equation (14), associated with the Ising variable exchange. We have used the values of the liquid cell mass,  $m = 1$ , and gravity acceleration,  $g = 10$ .

3. Calculate the transition probability  $W(\mathbf{x}_i \rightarrow \mathbf{x}_{i+1})$  according to equation (13). We have set the “Monte Carlo time” value at  $\tau = 1$ , and in our simulation, the product of the Boltzmann constant with the temperature has the value  $kT = 50$ .
4. The probabilistic nature of the spin exchange is realized via drawing a random number  $R$  that is uniformly distributed between zero and unity.
5. If  $R > W(\mathbf{x}_i \rightarrow \mathbf{x}_{i+1})$ , then exchange the spin cells. When a liquid particle is moved from the initial liquid layer (i.e.,  $h_i \in \{0, \dots, 9\}$ ), its position should always be refilled by liquid. This simulates the liquid absorbing from a nonexhaustive liquid reservoir.
6. The spin configuration obtained in this way at the end of step 5 is counted as a new configuration, and we then return to step 1.

After an adequate number of repeats, we can analyze the resulting configurations saved to obtain actual numerical data and the graphs of the system such as the total liquid absorbed and the sum of the total energy changes.

### 3.4 The Dynamic Interpretation of the Model

Apparently, the evolving configurations  $\mathbf{x}_i \rightarrow \mathbf{x}_{i+1}$  in the algorithm differ only by an exchange of a couple spins. That is why the physical properties of these neighboring states of the system are very strongly correlated. This correlation is the theoretical basis for the application of the Monte Carlo methods with *importance sampling* to the simulation of dynamic processes [16, 17, 34, 37]. The dynamic interpretation of the method is based on the association of a time  $t$  with the subsequent configuration  $\mathbf{x}_i \rightarrow (\mathbf{x}, t)$ . The time scale is often normalized into a relative unit, during which  $N$  spin exchange trials are performed. The time unit is called 1 MCS (Monte Carlo step per particle) [34].

For the probability distribution function in equation (15),  $P(\mathbf{x}, t)$  at time  $t$ , a configuration  $\mathbf{x}$  occurs in the Monte Carlo process that satisfies the Markovian master equation [38]:

$$\frac{dP(\mathbf{x}, t)}{dt} = - \sum_{\mathbf{x}'} W(\mathbf{x} \rightarrow \mathbf{x}') P(\mathbf{x}, t) + \sum_{\mathbf{x}'} W(\mathbf{x}' \rightarrow \mathbf{x}) P(\mathbf{x}', t). \quad (16)$$

In this equation, the first sum on the right-hand side represents all the processes that move the system away from the state  $\mathbf{x}$ . The second sum contains all the reverse events and leads to an increase of the probability  $P(\mathbf{x}, t)$  of finding the system in the configuration  $\mathbf{x}$ . In the case of thermal equilibrium, these two sums cancel each other, and we have  $dP_{eq}(\mathbf{x}, t)/dt = 0$ , where  $P_{eq}(\mathbf{x})$  is the steady-state distribution of the master equation (16).

In general, the time associated with the *importance sampling* procedure cannot be related to the physical time by which a real system evolves. The reason is that the time evolution in a real system is governed by the deterministic equations, not the stochastic master equation (16). But for the Ising Hamiltonian (12), the stochastic kinetics provided by (16) could be interpreted physically in terms of a very weak coupling of the spins to a heat bath, which induces random spin exchanges in the system [34].

#### 4. Predictions by the Ising Model

##### 4.1 Influences of the Fiber Orientation

In the simulation, we first investigated the influence of fiber orientation on the dynamics of liquid wetting and wicking into a fibrous mass. We varied the fiber declination  $\beta$  from the vertical axis  $H$  with the step of  $10^\circ$ , so the simulation was carried out for 11 different fibrous systems with  $\beta = 0^\circ, 10^\circ, 20^\circ, \dots, 90^\circ$ , plus  $\beta = 45^\circ$ . After each Monte Carlo step per cell (MCS), the following outputs were collected, such as the number or the mass  $m_A$  of wicked liquid particles, the liquid particles above the original liquid surface, and the changes of the total system energy  $\Delta E$ . The simulation was terminated after 600 MCS, and information of each new configuration was saved for further analysis.

Results of this process are provided in Figure 5; each picture is a paired wetting pattern of a cross section with a side view and a top view of the fibrous mass at a given  $\beta$  value. The horizontal cross sections are all cut at the distance of 100 cells from the liquid surface.

We find two extremes from the pictures. The first is the one vertical to the  $W-L$  plane or  $\beta = 0^\circ$ , where the ascending liquid moves at a highest rate but is most scattered. The other one is in parallel with the  $W-L$  plane or  $\beta = 90^\circ$ , with the lowest wetting rate, but the liquid pattern is most heavily aggregated (also see Fig. 6a).

From Figure 5, one can intuitively evaluate the volume of the liquid wicked into a fiber mass. Yet from Figure 6a, it is clear that after a short time (i.e.,  $MCS < 200$ ), the absorbed liquid body in general is more voluminous for a smaller angle  $\beta$  because, apparently, the fiber assemblies with smaller  $\beta$  values start with greater wicking rates, and therefore the liquid climbs faster. Nevertheless, this trend remains true in our calculation only for those with  $\beta \geq 20^\circ$ , whereas when  $\beta < 20^\circ$ , the climbing of the liquid will stagnate and become independent of the time; the smaller the  $\beta$  value, the earlier the climbing stops.

The discussions above reveal that there will be one or a range of optimal combinations of  $\beta$  and MCS at which the fiber mass will absorb a maximum amount of liquid, a result of the optimal wicking rate and wicking duration, as illustrated in Figure 6b; when  $\beta = 20^\circ$ , the greater the MCS value and the more liquid absorbed into the specimen.

##### 4.2 The Wicking Rate $K$

To evaluate the wicking rate  $K$ , we have plotted the time derivation of the wicked liquid mass,  $dm_A/dt$ , against the

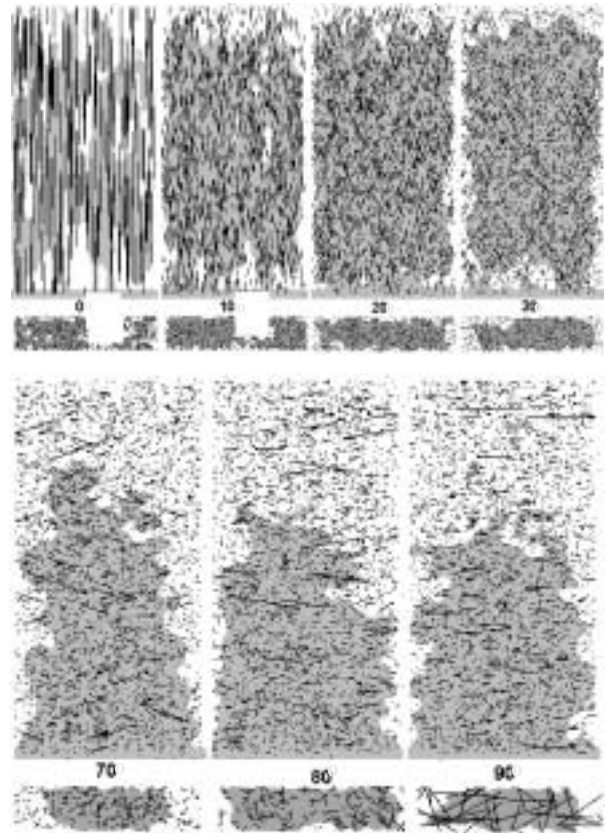


**Figure 5.** Wetting patterns from both vertical and horizontal cross sections of a fiber mass at different orientation angles  $\beta$  after 600 MCS (Monte Carlo step per particle). The fibers in the individual samples have strictly identical declination  $\beta$ . From the left- to the right-hand side, the  $\beta$  values are  $0^\circ, 10^\circ, 20^\circ, 30^\circ, 70^\circ, 80^\circ$ , and  $90^\circ$ , as denoted in each sample. Only those fibers that lie in the cross-section plane are depicted in full length with the corresponding declination angle  $\beta$ . The fiber system is uniformly random.

reciprocal value of the mass  $\frac{1}{m_A}$  with different  $\beta$  values in Figure 7. We mentioned earlier that the value of  $K$  could be determined from the slope of the plot, as indicated in equation (9). In general, a wicking rate can be defined as  $K = tg\alpha$ , where  $\alpha$  is the slope of the plot.

It is clear from Figure 7a-c that a fibrous mass with a smaller  $\beta$  value does yield a higher slope or a greater wicking rate  $K$ . However, according to equation (9), when other parameters are given, this  $dm_A/dt$  against  $\frac{1}{m_A}$  should be a straight line. The results of the simulation in Figure 7, which is consistent with experimental practice, demonstrate otherwise. In reality, the wicking rate  $dm_A/dt$  cannot maintain a constant because, among other factors, the liquid weight will slow down and eventually stop the wicking process (i.e., the wicking rate  $dm_A/dt$  decreases mono-

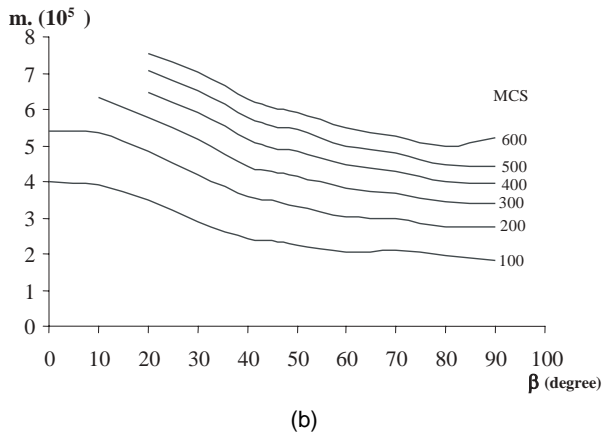
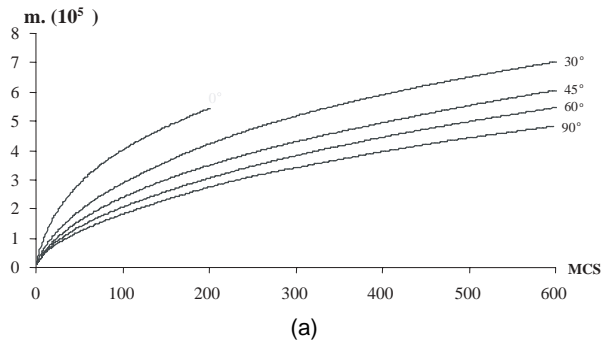


**Figure 6.** (a) The dependency of liquid mass wicked into a specimen on MCS (Monte Carlo step per particle) at a different fiber orientation angle  $\beta$ . (b) The dependency of liquid mass wicked into a specimen on orientation angle  $\beta$  after different MCS values.

tonically with time until zero). This, on the other hand, provides strong evidence for validating our computer simulation method.

A more complete analysis of the relationship between wicking rate  $K$  and the fiber mass orientation angle  $\beta$  based on the simulated data is summarized in Figure 8. We see that the connection between the two is also nonlinear, with a rapid decrease of wicking rate  $K$  in the interval  $\beta \in (0^\circ, 30^\circ)$ , while the rest of the graph,  $\beta > 30^\circ$ , shows a constant or even slight increase of  $K$ .

#### 4.3 Total System Energy Exchange $\Delta E$

Figure 9a is a plot of the total system energy changes  $\Delta E$ , along with the time MCS at different angles  $\beta$ . These curves do not reach their asymptotic behavior of the steady states that would be parallel with the MCS axis, with few changes in  $\Delta E$ .  $\Delta E < 0$  indicates that the wicking process is an exothermal process. The magnitude of  $|\Delta E|$  increases monotonically with the MCS value as more spin

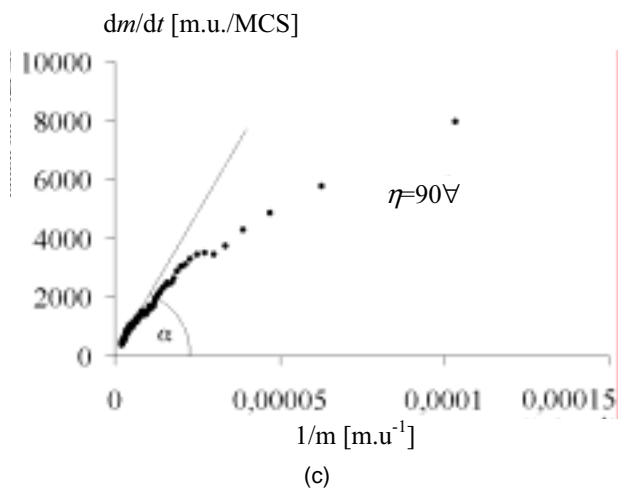
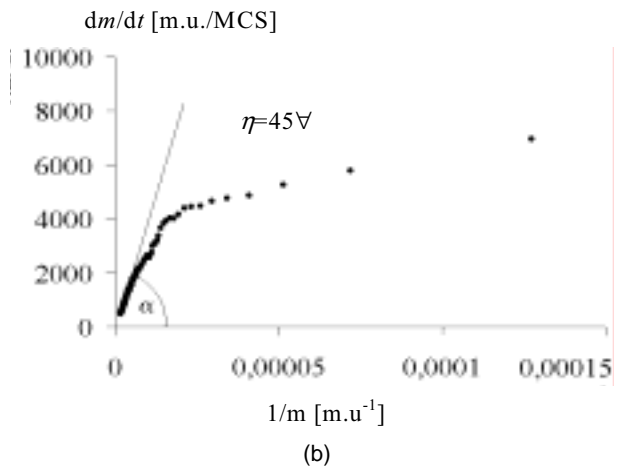
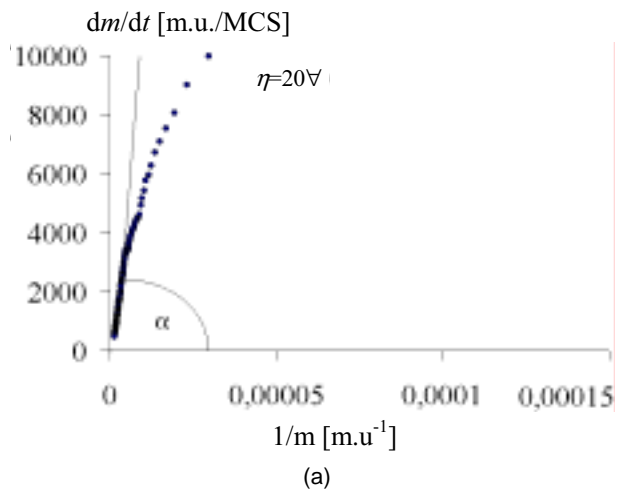


**Figure 7.** Time derivation of wicked liquid mass  $d_{m_A}/dt$  against the reciprocal mass  $1/m_A$ : (a) fiber orientation  $\beta = 20^\circ$ , (b) fiber orientation  $\beta = 45^\circ$ , and (c) fiber orientation  $\beta = 90^\circ$

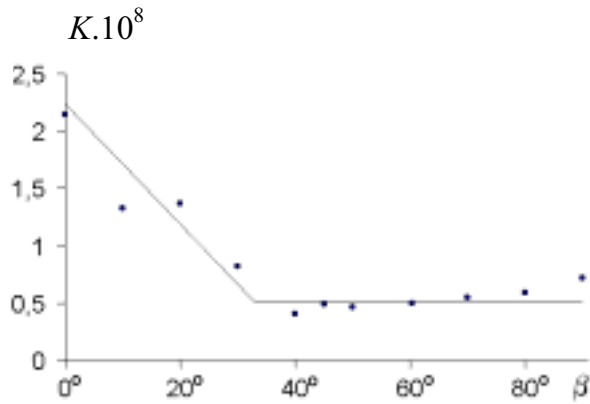


**Figure 8.** The generalized wicking rate  $K$  versus fiber orientation angle  $\beta$

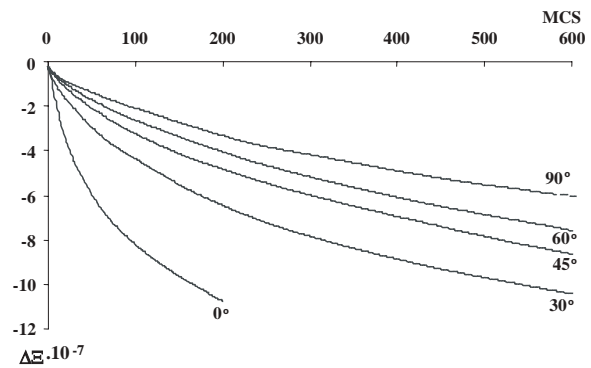
exchanges are conducted or more liquid is absorbed into the fiber mass. Similar to the case in Figure 6, a dependency of  $|\Delta \Xi|$  on  $\beta$  is revealed. Likewise, the optimal combination of  $\beta$  and MCS for extreme values of  $|\Delta \Xi|$  can be determined in Figure 9b.

Finally, it should be noted that a major problem in our method is the presence of the anisotropy generated due to the underlying cubic lattice, but this effect is minimized by a relatively high value of  $kT$ . Furthermore, up to now, the Lucas–Washburn theory is still the most widely accepted method for evaluating the wicking rate in textile materials. Nonetheless, there are a few discrepancies between the theory and the experimental data. It seems that the major problem lies in the dissimilarity between the geometry of liquid bodies in the “Lucas–Washburn tube” and in the actual fibrous mass. The area filled by the liquid on a cross section of a “Lucas–Washburn tube” is constant with a clear-cut fluid surface in the vicinity of the summit of the liquid body, while the liquid body in a capillary of the fibrous mass has a complex pyramidal shape. So once again, the Lucas–Washburn theory is applicable only at an infinitesimal height of liquid ascending.

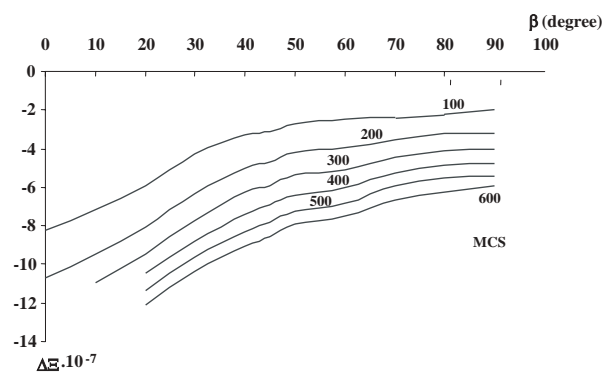
### 5. Conclusions

By replacing the wicking height with liquid mass uptake, the original Lucas–Washburn equation governing the ascension of a liquid wicking in a hanged fibrous sample dipped into the liquid reservoir is extended into the case of the radial expansion of the wicking liquid originating at the center of a flat sample. Also, it is shown that by using the liquid mass uptake  $m_A$ , the Lucas–Washburn equation can be transformed into a new form,

$$\frac{dm_A}{dt} = \frac{K}{m_A} - L,$$



(a)



(b)

**Figure 9.** (a) Total system energy change  $\Delta \Xi$  versus MCS (Monte Carlo step per particle) at different fiber orientation angle  $\beta$  and (b) total system energy change  $\Delta \Xi$  versus fiber orientation angle  $\beta$  after different MCS

with clearer physical meaning and more ease for discussion.

However, there are problems with Lucas–Washburn-type theories. First, the assumed cylindrical capillary tubes are far from the real cases. Also, because of the increasing mass of the ascending liquid in a vertical sample, the wicking rate is in fact a variable, not a constant, as assumed in the theories. Furthermore, this kind theory is unable to deal with the influences of several key system parameters, including the fiber orientation and fiber volume fraction.

We have hence presented a 3-D stochastic method based on the Ising model with Kawasaki dynamics on a cubic lattice to obtain the shape of a liquid body wicked into a fibrous material with known fiber orientations. Computer simulations based on this method realistically and quantitatively depict the dynamic liquid ascending wicking process. Moreover, a parametric study has been conducted in this article to examine the influences of the important factors involved in the simulation.

The results simulated, for instance, indicate that the relationship between the fiber orientation  $\beta$  and the generalized wicking rate  $K$  is nonlinear, and a greater wicking rate  $K$  can be achieved for the structures with fiber orientation  $\beta$  smaller than  $30^\circ$  from the axis perpendicular to the original liquid surface.

The effects of  $\beta$  on the total liquid absorption are not monotonic; a smaller  $\beta$  leads to a greater wicking rate  $K$  as stated above or a quicker liquid wicking process. The wicking process, however, will stagnate as time increases, whereas a greater  $\beta$  results in a slower wicking rate, but the wicking process can proceed longer. An optimal condition can be explored.

It is obviously necessary to validate our simulations with experimental data carried out with real fibrous materials. The experimental study, in fact, has been completed and will be reported in another paper. The study of the influence of mixed fiber orientations in a fiber mass, as well as the relationship between the generalized wicking rate and the fiber volume fraction, is the next logical goal of this research.

An anisotropy of liquid transport in fibrous layers is of high interest for producers of disposable products such as diapers and feminine hygiene. The liquid distribution in such commodities has to be selective so as to protect consumers against side outpour, which is achieved by the so-called acquisition layers, whose function could be controlled by using the wicking rate–fiber orientation relationship.

As the last concluding remark, we highlight the effect of individual fiber morphology. A proper shape of the fiber cross section can effectively improve the liquid transport and the liquid film stability along isolated fibers. The well-known example of this phenomenon is the Rayleigh instability of liquid films on cylindrical fibers.

## 6. Acknowledgment

The authors are thankful to Dr. Gupta, B. S. from North Carolina State University for useful comments and remarks to this work, and Ing. Eva Kostakova from the Technical University of Liberec for her technical aid concerning the figures.

## 7. References

- [1] Hentschel, H. G. E. 1994. *Encyclopaedia of applied physics: Nonhomogeneous flows*. Vol. 11. New York: VCH Publishers.
- [2] Young, T. 1972. *Miscellaneous works*. Vol. 1. Edited by G. Peacock. New York: Johnson Reprint Corporation.
- [3] De Laplace, P. S. 1806. *Mechanique celeste*. Supplement to Book 10. Paris: Durat.
- [4] Lamb, H. [1879] 1945. *Hydrodynamics*. Reprint, New York: Dover.
- [5] Huh, C., and L. E. Scriven. 1971. Hydrodynamic model of steady movement of a solid/liquid/fluid contact line. *Journal of Colloid and Interface Science* 35:85-101.
- [6] Dussan, V. E., and S. Davis. 1974. On the motion of a fluid–fluid interface along a solid surface. *Journal of Fluid Mechanics* 65:71-95.
- [7] Brochard, F., and P. G. de Gennes. 1984. Spreading laws for liquid polymer droplets—interpretation of the foot. *Journal de Physique (Paris) Lettres* 45 (12):L597-L602.
- [8] de Gennes, P. G. 1985. Wetting: statics and dynamics. *Reviews of Modern Physics* 57 (3, pt. 1): 826-63.
- [9] Lucas, R. 1918. Ueber das Zeitgesetz des kapillaren Aufstiegs von Flüssigkeiten. *Kolloidn Zhurnal* 23:15-22.
- [10] Washburn, E. W. 1921. The dynamics of capillary flow. *Physical Review* 17:273-83.
- [11] Chatterjee, P. K. 1985. *Absorbency*. Amsterdam: Elsevier.
- [12] Pillai, K. M., and S. G. Advani. 1996. Wicking across a fiber-bank. *Journal of Colloid and Interface Science* 183:100-10.
- [13] Hsieh, Y. L. 1995. Liquid transport in fibrous assemblies. *Textile Research Journal* 65:299-307.
- [14] Hirt, D. G., K. L. Adams, R. K. Prud'Homme, and L. Rebenfeld. 1987. In-plane radial fluid flow characterization of fibrous materials. *Journal of Thermal Insulation* 10:153-72.
- [15] Lukas, D., and V. Soukupova. 1999. Recent studies of fibrous materials wetting dynamics. In *INDEX 99 Congress*, Geneva, Switzerland.
- [16] Manna, S. S., H. J. Herrmann, and D. P. Landau. 1992. A stochastic method to determine the shape of a drop on a wall. *Statistical Physics* 66:1155-63.
- [17] Lukkarinen, A. 1995. Mechanisms of fluid spreading: Ising model simulations. *Physical Review E: Statistical Physics, Plasma, Fluids, and Related Interdisciplinary Topics* 51:2199-2202.
- [18] Starov, V. M., S. A. Zhdannov, S. R. Kosvinste, V. D. Sobolev, and M. G. Velarde. 2003. Effect of interfacial phenomena on dewetting in dropwise condensation. *Advances in Colloid and Interface Science* 104:175-90.
- [19] Lukas, D., and N. Pan. 2003. Wetting of a fiber bundle in fibrous structures. *Polymer Composites* 24:314-22.
- [20] Lukas, D., E. Glazirina, and N. Pan. 1997. Computer simulation of liquid wetting dynamics in fiber structures using the Ising model. *Journal of the Textile Institute* 88 (2):149-61.
- [21] Zhong, W., X. Ding, and Z. L. Tang. 2002. Analysis of fluid flow through fibrous structures. *Textile Research Journal* 72:751-55.
- [22] Zhong, W., X. Ding, and Z. L. Tang. 2001. Modeling and analyzing liquid wetting in fibrous assemblies. *Textile Research Journal* 71:762-66.
- [23] Gupta, B. S. 1997. Some recent studies of absorbency in fibrous nonwovens, XXV. In *International Nonwovens Colloquium*, Brno, Czech Republic.
- [24] Miller, B., and H. L. Friedman. 1992. Adsorption rates for materials under compression. *Tappi Journal*, December, 161-65.
- [25] Berg, J. C. 1989. The use of single-fibre wetting measurements in the assessment of absorbency. In *Nonwovens advanced tutorial*, edited by F. T. Albin and L. V. Tyrone. Atlanta, GA: TAPPI Press.
- [26] Landau, L. D., and E. M. Lifshitz. 1988. *Theoretical physics: Vol. 6. Hydrodynamics*. Moscow: Nauka.
- [27] Ford, L. R. 1933. *Differential equations*. New York: McGraw-Hill.
- [28] Hsieh, Y. L. 1995. Liquid transport in fibrous assemblies. *Textile Research Journal* 65:299-307.
- [29] Miller, B., and S. H. Jansen. 1982. Wicking of liquid in nonwoven fiber assemblies: Advances in nonwoven technology. In *10th Technical Symposium*, New York, pp. 216-26.
- [30] Everet, D. H., J. M. Haynes, and R. J. Miller. 1978. Kinetics of capillary imbibition by fibrous materials. In *Fibre-water interactions in papermaking*, edited by the Fundamental Research Committee. London: Clowes.
- [31] Metropolis, N., A. W. Rosenbluth, M. N. Rosenbluth, A. Teller, and E. Teller. 1953. Equation of state calculation by fast computing machines. *Journal of Chemical Physics* 21:1087-92.
- [32] Binder, K., ed. 1986. *Monte Carlo methods in statistical physics*. 2nd ed. Berlin: Springer.
- [33] Müller-Krumbhaar, H., and K. Binder. 1973. Dynamical properties of the Monte Carlo method in statistical mechanics. *Journal of Statistical Physics* 8:1-24.

- [34] Binder, K., and D. W. Heermann. 1997. *Monte Carlo simulation in statistical physics: An introduction*. 3rd ed. Berlin: Springer.
- [35] Wibel, E. R. 1979. *Stereological method*. Vol. 1. London: Academic Press.
- [36] Kawasaki, K. 1972. Kinetics of Ising models. In *Phase transitions and critical phenomena*, edited by C. Domb and M. S. Green. Vol. 2. New York: Academic Press.
- [37] Herrmann, H. J. 1986. Geometrical cluster growth models and kinetic gelation. *Physics Reports* 136:153-224.

**D. Lukas** is a professor at the Technical University of Liberec, Liberec, Czech Republic.

**V. Soukupova** is a PhD student at the Technical University of Liberec, Liberec, Czech Republic.

**N. Pan** is a professor in the Division of Textiles and Clothing, Biological and Agricultural Engineering Department, University of California, Davis.

**D. V. Parikh** is a scientist at the South Regional Research Center, New Orleans, Louisiana.